Supporting information

Self-Polymerized Dopamine as an Organic Cathode for Li- and Na-Ion Batteries

Tianyuan Liu,‡[a] Ki Chul Kim,‡[b] Byeongyong Lee,[a] Zhongming Chen,[c] Suguru Noda,[c] Seung Soon Jang,[b*] Seung Woo Lee[a*]

[a] G. W. Woodruff School of Mechanical Engineering, Georgia Institute of Technology, Atlanta, Georgia 30332-0405,

United States

[b] Computational NanoBio Technology Laboratory, School of Materials Science and Engineering, Georgia Institute of Technology, Atlanta, Georgia 30332-0245, United States

[c] Department of Applied Chemistry, Waseda University, 3-4-1 Okubo, Shinjuku-ku, Tokyo 169-8555, Japan

‡ These authors have contributed equally.
[*] Corresponding Author: seungsoon.jang@mse.gatech.edu, seung.lee@me.gatech.edu

DFT Calculations: All the calculations to compute the redox potentials of molecules were performed by the Jaguar software with the PBE0 level of theory and 6-31G+(d,p) basis set.[1,2] First of all, we geometrically optimized the 5,6-dihydroxyindole and 5,6-indolequinone monomers and their oligomers such as dimer and trimer. The vibrational frequency calculations with the same level of theory and basis set were further performed to compute the Gibbs free energies at 298 K in the vacuum. The solvation free energy calculations were finally performed using Poisson-Boltzman implicit solvation model to evaluate the contribution of the solvation free energies to the free energies. In the solvation free energy calculations, a dielectric constant of 16.14 was used to reliably describe the polarity of the solvent mixture in our systems.

The thermodynamic cycle, which was used to predict the redox potentials of the molecules, is described elsewhere.[3] The redox potential (ΔE^{red}) of a molecule within the solvent mixture with respect to a Li/Li$^+$ reference electrode can be predicted by

$$\Delta E^{red} = \frac{-\Delta G^{soln}}{nF} - 1.44V$$

where ΔG^{soln} is the difference in the Gibbs free energy in solution during the reduction, *n* is the number of electrons transferred, and *F* is the Faraday constant. The constant 1.44 V indicates the redox potentials of the Li/Li$^+$ reference electrode. The computed redox potentials of the molecules are listed in Table S1. The electronic properties such as the highest occupied molecular orbital (HOMO) and lowest unoccupied molecular orbital (LUMO) energy levels of the molecules were also computed to investigate the correlations with their redox potentials.

Sample preparation: Few-walled carbon nanotubes (FWNTs) (6–10 nm diameter, 0.4 mm length, 99 wt% purity, triple-walled on average) were synthesized by CVD method in a single fluidized bed reactor.[4, 5] Dopamine (Sigma-Aldrich) and FWNTs were mixed at different mass ratio (*i.e.* 1:1, 2:1, 4:1 and 8:1) in 1.2 mg/mL 2-amino-2-hydroxymethylpropane-1,3-diol (Tris, Aldrich) aqueous solution. The solutions were stirred for 6 ~ 18 h, then, were vacuum filtered using a filtration membrane with 0.1 μm pore size. After drying at 70 ^{o}C under vacuum overnight, a piece of free-standing hybrid film was obtained. Pristine FWNT films were obtained by vacuum filtering the aqueous dispersion of FWNTs. Pristine PDA particles were also prepared by the similar process by stirring dopamine in weak alakline soltuion (pH=8.5) for 6 h without adding FWNTs.

Characterization: The microstructures and morphologies of pristine FWNT films and various hybrid films were characterized by a scanning electron microscope (SEM, Hitachi SU8010, operated at 10 kV). The EDX mapping was performed using Hitachi SU8230 equipped with an EDX detector (Oxford Instruments) at 10 kV. X-ray photoelectron spectroscopy (XPS, Thermal Scientific K-alpha XPS instrument) was employed to analyze the chemical composition. The high-resolution C 1s, N 1s and O 1s peaks were fitted by the software XPSPEAKS 4.1. Electrical conductivities of various FWNT films were measured by a standard four-point probe configuration (Signatone). The UV-vis spectroscopy was conducted by sonicating a small piece of the composite film in water for 1 h, the supernatant was used for UV-vis measurement. In comparison, fresh dopamine aqueous solution was prepared just before UV-vis measurement to avoid the possible oxidation.

Electrochemical Measurements: Swagelok-type cells were used for the electrochemical measurements. For Li-cell tests, 1 M $LiPF_6$ in a mixture of ethylene carbonate (EC) and dimethyl carbonate (DMC) (3:7, volume ratio, BASF) was used as an electrolyte and two pieces of Celgard 2500 as separators. The voltage window for Li-ion batteries was controlled in the range of 1.5-4.5 V vs. Li. For Na-cell tests, 1 M $NaPF_6$ in EC/DMC (3:7, volume ratio, BASF) was used as electrolyte, and a piece of glass fiber (VWR International) was used as separator. The Na-cells were tested in the voltage range from 1.3 to 4.2 V vs. Na. All of the cells were assembled in an Argon filled glovebox (MBraun, O_2 < 0.1 ppm and H_2O < 0.1 ppm). The thickness of the hybrid films is 97 μm for PDA 39 wt%, and 54 μm for PDA 53 wt%. Current densities were controlled from 0.05 to 50 A/g during the galvanostatic tests and at the end of each charging or discharging process, the voltage was held for 30 min at either 4.5 V or 1.5 V vs. Li (4.2 V or 1.3 V vs. Na). The conventional cycling test was conducted by repeatedly charging and discharging the cell at 0.25 A/g for 100 cycles. The cycling test with potentiostatic holding was held at 4.5 V or 1.5 vs. Li (4.2 V or 1.3 V vs. Na) for 5 min at the end of charge/discharge process. The accelerated cycling test was conducted following our previous reports.[6] Briefly, the charge or discharge capacity was obtained from a low current density of 0.1 A/g and at the end of each charge or discharge process, the cell was held at 4.5 or 1.5 V vs. Li for 30 min. Between each data point, the cell was cycled at a high current density of 10 A/g for 99 cyces (1-1,000th cycle) or 499 cycles (1,100th-10,000th cycle).

Self-discharge course and the ex-situ XPS measurement: The hybrid electrodes were charged or discharged to target voltage at 0.1 A/g and held at costant voltage (4.5, 3.5, 1.5 V vs. Li) for 60 min. After hold process, the cell was rested at open-circuit condition for ~18 h and the voltage was recorded with time. After the voltage of the cell was stabalized for ~18 h, the cell was

dissembled and the electrode was washed with DMC for several times, and vacuum dried at 70 °C for overnight before the XPS measurement.

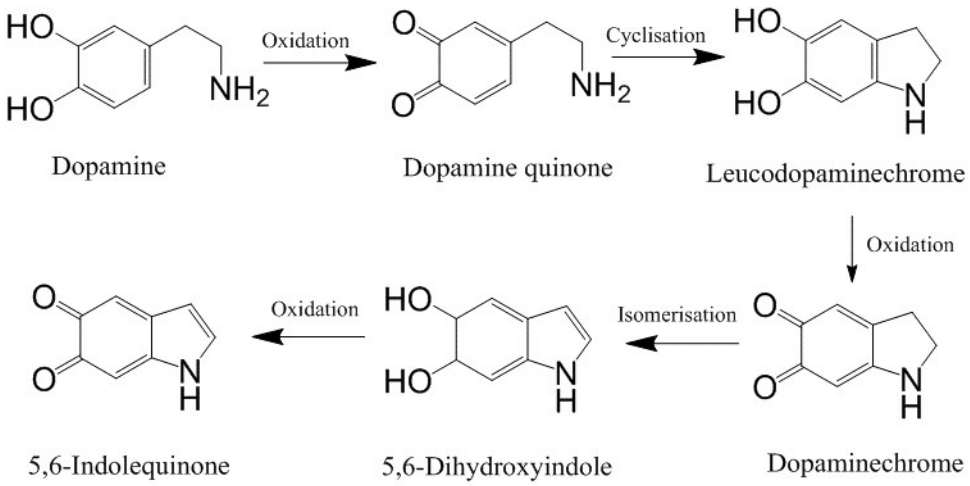

Scheme S1. Contemporary reaction mechanism of polydopamine from dopamine including various intermediate species, which is modified from the previous study.[7]

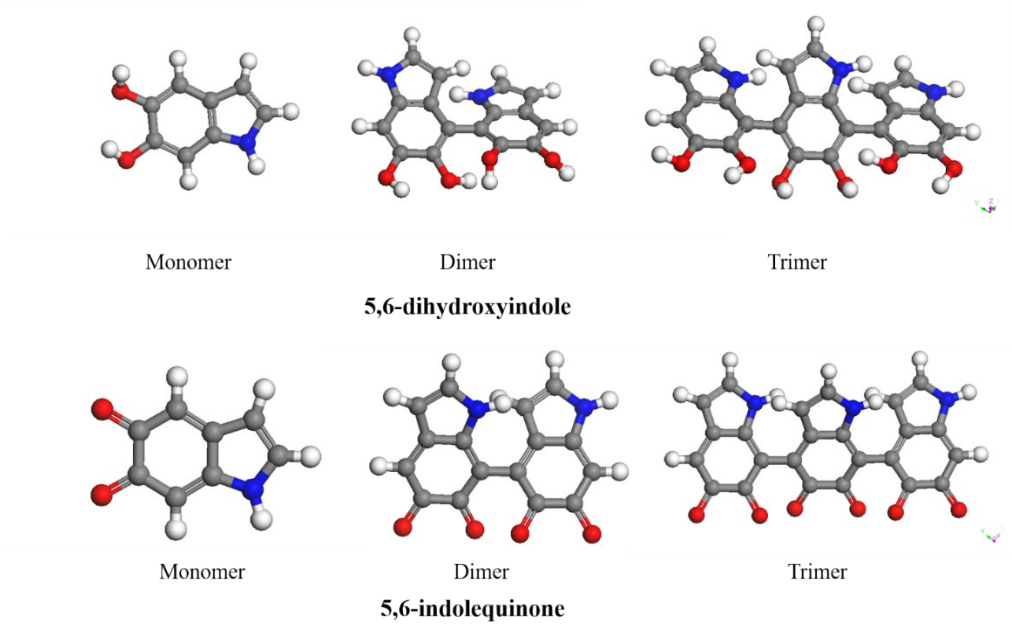

Scheme S2. The molecular structures of 5,6-dihydroxyindole and 5,6-indolequinone monomers and their oligomers.

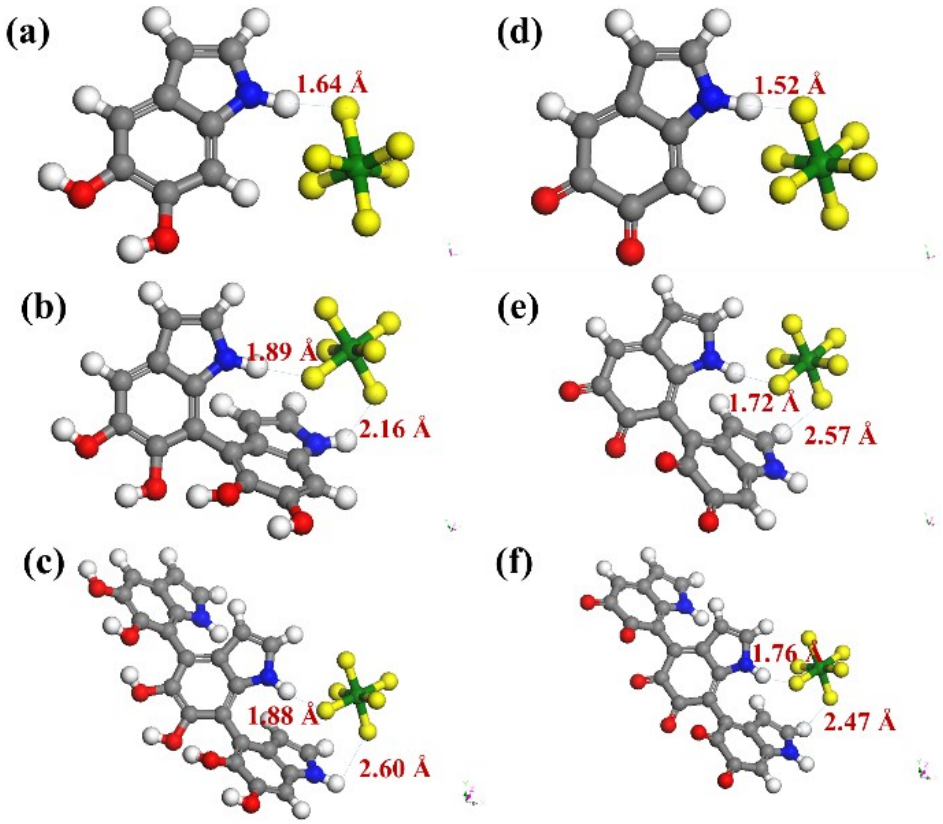

Scheme S3. Geometrically optimized structures for the monomers and oligomers of 5,6-dihydroxylindole and 5,6-indolequinone with PF_6^-. The shortest distances of P-H in Å are shown in red. Gray, white, blue, red, green, and yellow in color depict carbon, hydrogen, nitrogen, oxygen, phosphorus, and fluorine, respectively.

Table S1. The calculated redox potentials of 5,6-dihydroxyindole and 5,6-indolequinone monomers and their oligomers illustrated in Figure 1.

Molecule		Redox potential (V *vs.* Li/Li^+)
5,6-dihydroxyindole	**Monomer**	-0.26
	Dimer	0.11
	Trimer	0.27
5,6-indolequinone	**Monomer**	2.83
	Dimer	2.94
	Trimer	2.93

Table S2. The calculated redox potentials of 5,6-dihydroxyindole and 5,6-indolequinone monomers and their oligomers associated with the doping and de-doping process of anions.

Molecules		Calculated Redox Potential (V)	Electron affinity (kcal/mol)	HOMO (eV)	LUMO (eV)	HOMO-LUMO Gap (eV)
5,6-dihydroxyindole	Monomer	4.03	-100.9	-7.72	-3.85	3.87
	Dimer	3.82	-92.8	-6.27	-3.59	2.68
	Trimer	3.73	-91.9	-6.11	-3.55	2.56
5,6-indolequinone	Monomer	4.41	-114.2	-8.75	-5.76	2.99
	Dimer	3.97	-104.1	-7.32	-5.2	2.12
	Trimer	3.95	-106.0	-6.98	-5.10	1.88

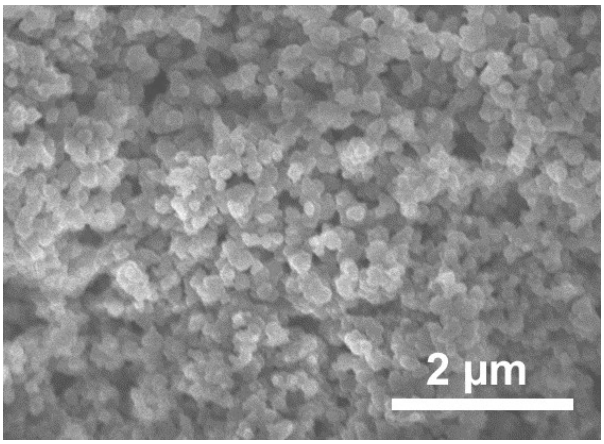

Figure S1. Scanning electron microscope (SEM) image of as prepared polydopamine (PDA) particles. The polydopamine (PDA) particles were prepared by directly stirring dopamine solution in weak alkaline solution (pH=8.5) for 6 h without using FWNTs as a template.

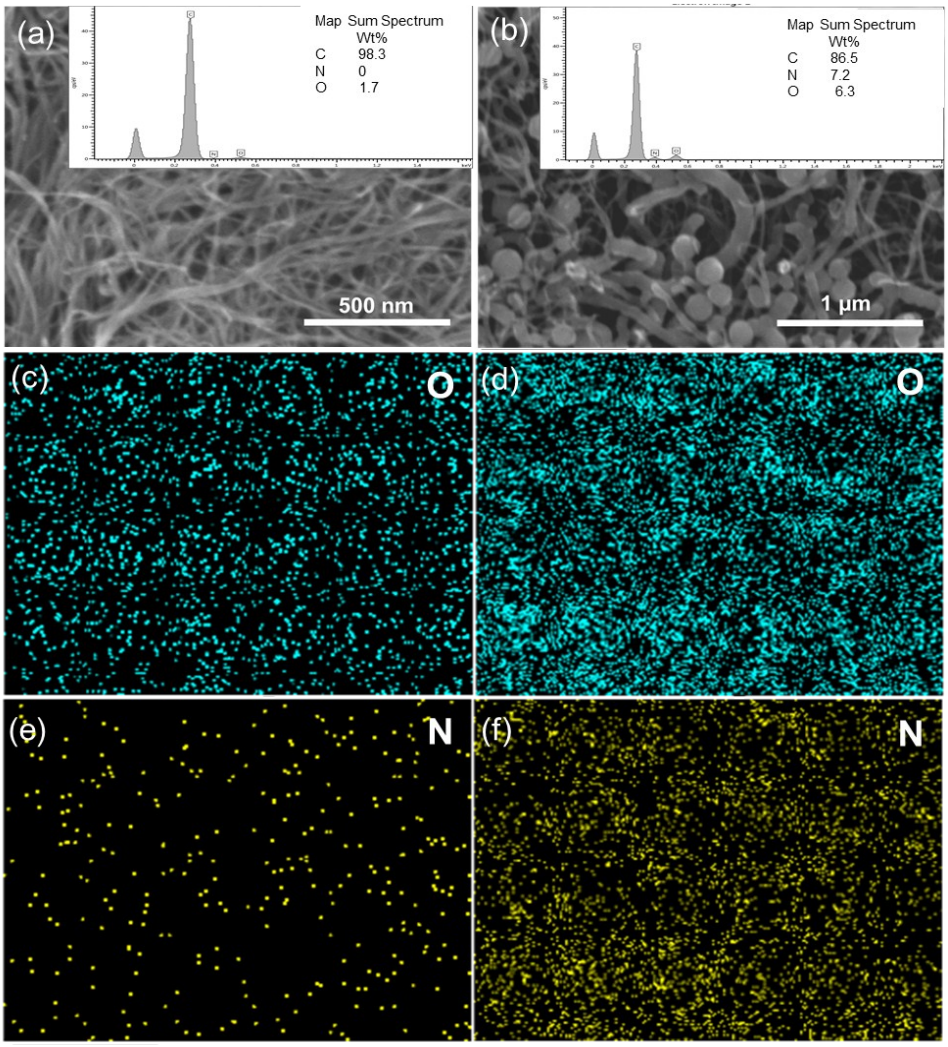

Figure S2. SEM images of (a) pristine FWNT film and (b) hybrid film (PDA-2, 53%) and corresponding EDX elemental mapping of (c,d) oxygen and (e,f) nitrogen.

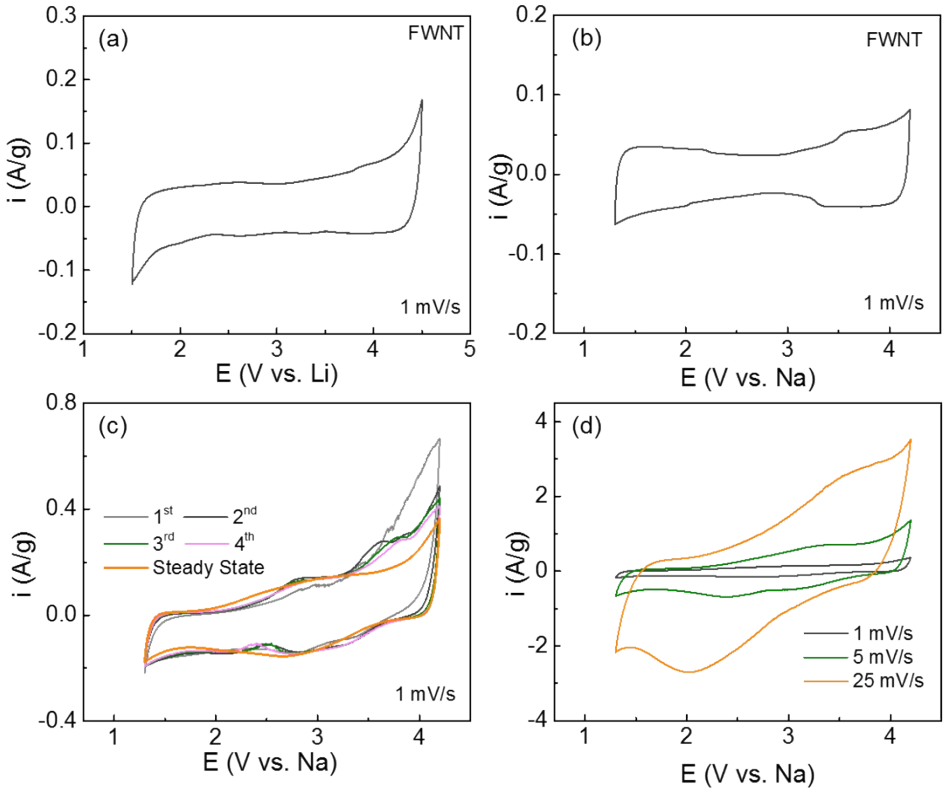

Figure S3. Cyclic voltammogram (CV) scans of the pristine FWNT electrodes 1 mV/s in (a) Li and (b) Na-cells. (c) The first four CV scans and (d) Rate-dependent CV scans of the hybrid electrode (PDA-2, 39 wt%).

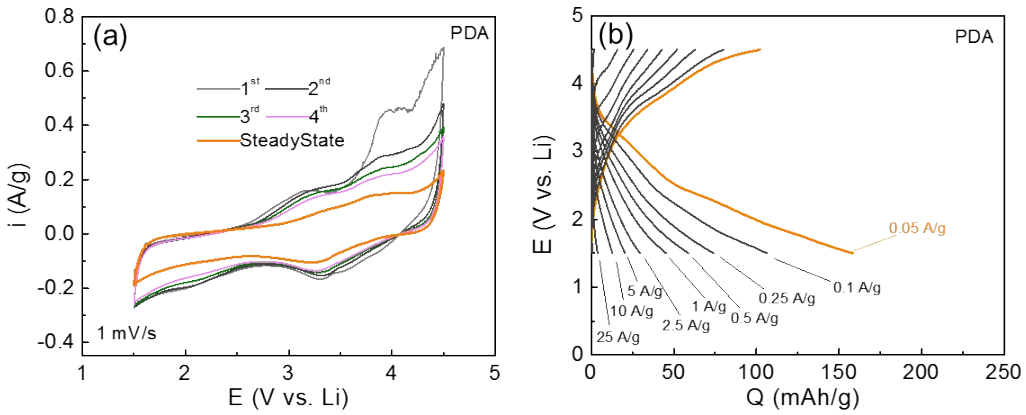

Figure S4. (a) Cyclic voltammetry (CV) measurement of pristine PDA and (b) rate-dependent galvanostatic charge-discharge profiles of the pristine PDA in Li-cells.

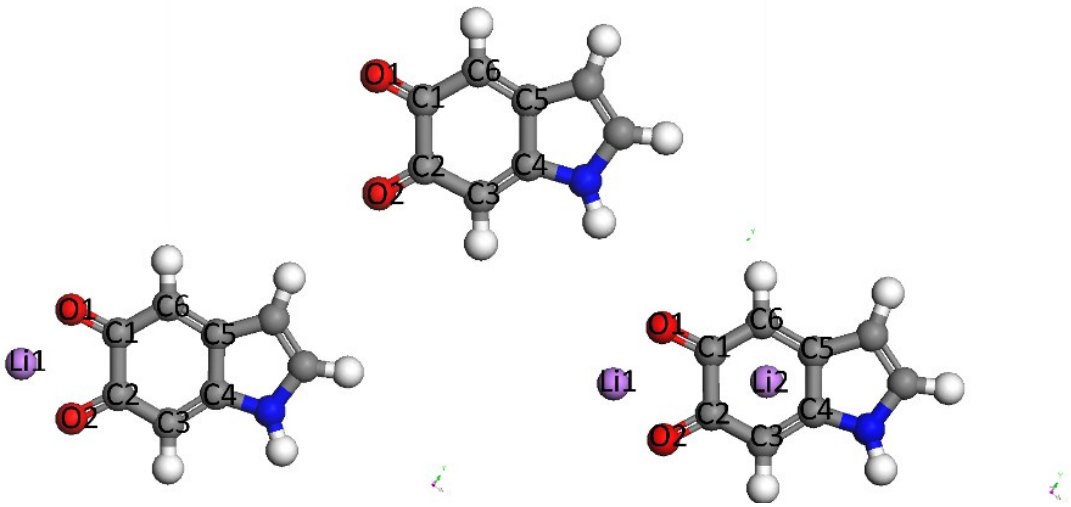

Figure S5. Change in the structure (PBE0 functional) as a function of the Li atoms binding with 5,6-indolequinone monomer.

Table S3. Change in the bonding distance and charge distribution (PBE0 functional) as a function of the Li atoms binding with 5,6-indolequinone monomer.

Bond Type	Distance (Å)			Atom	Charge		
	Without Li	With 1Li	With 2Li		Without Li	With 1Li	With 2Li
Li1-O1	-	1.81	1.79	Li1	-	0.51	0.46
Li1-O2	-	1.81	1.80	Li2	-	-	0.08
Li2-C1	-	-	2.31	O1	-0.37	-0.52	-0.58
O1-C1	1.22	1.28	1.30	O2	-0.39	-0.52	-0.59
O2-C2	1.22	1.28	1.29	C1	0.26	0.29	0.34
C1-C2	1.57	1.50	1.50	C2	0.25	0.31	0.38
C2-C3	1.46	1.41	1.41	C3	-0.26	-0.32	-0.34
C3-C4	1.36	1.38	1.42	C4	0.25	0.22	0.32
C4-C5	1.48	1.45	1.42	C5	-0.02	-0.07	0.01
C5-C6	1.36	1.39	1.43	C6	-0.23	-0.27	-0.30
C6-C1	1.46	1.41	1.41				

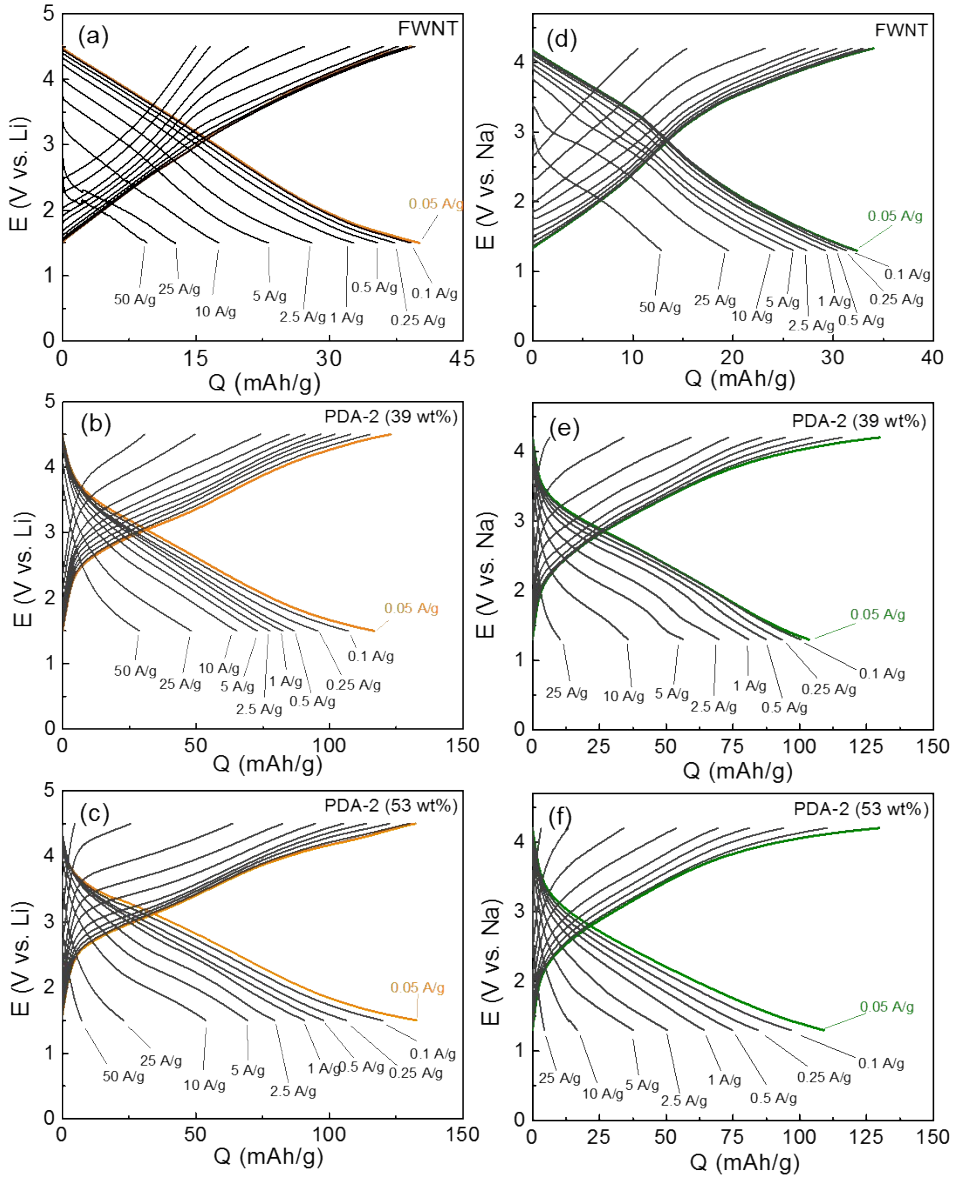

Figure S6. Rate-dependent galvanostatic charge-discharge profiles of the pristine FWNT electrodes in (a) Li- and (d) Na-cells. Rate-dependent galvanostatic charge-discharge profiles of the hybrid electrodes (PDA-2) in Li-cells (b for 39 wt% and c for 53wt%) and Na-cells (e for 39 wt% and f for 53wt%).

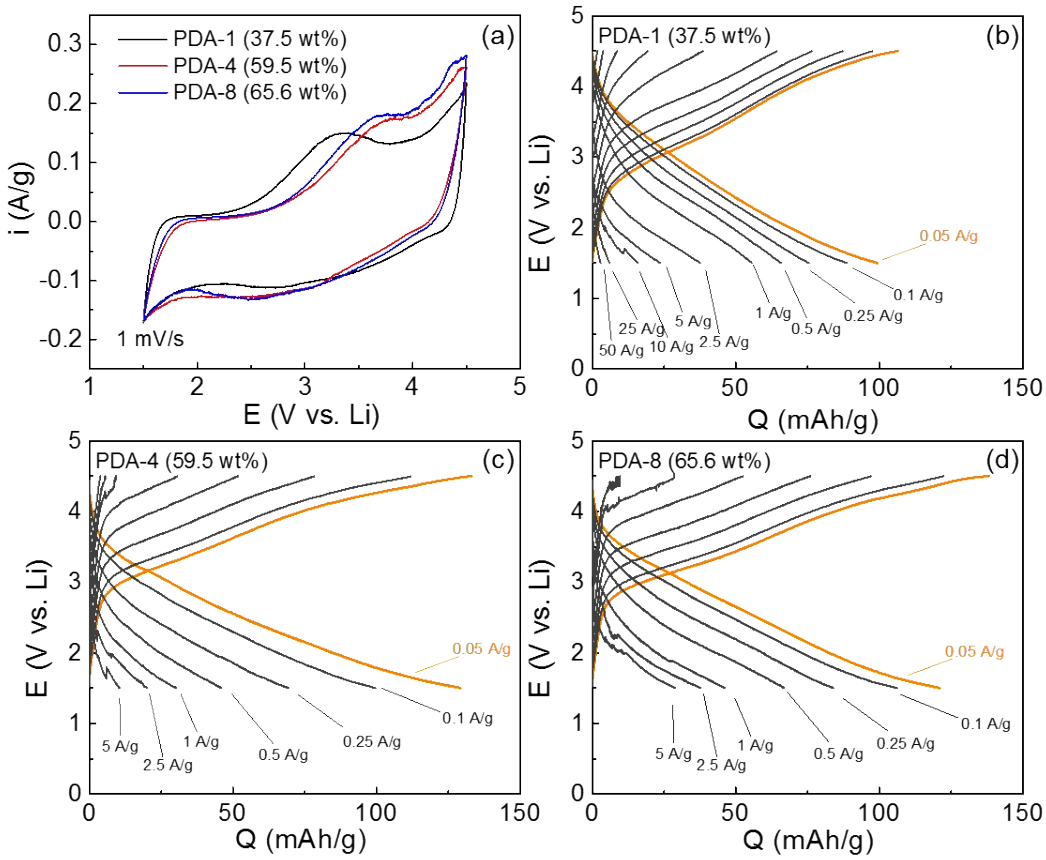

Figure S7. (a) Cyclic voltammetry (CV) measurement of the hybrid electrodes (PDA-1, 4, 8, 18 h stirring) in Li-cells. Rate-dependent galvanostatic charge-discharge profiles of the hybrid electrodes in Li-cells for (b) PDA-1, 37.5 wt%, (c) PDA-4, 59.5 wt%, (d) PDA-8, 65.6 wt%.

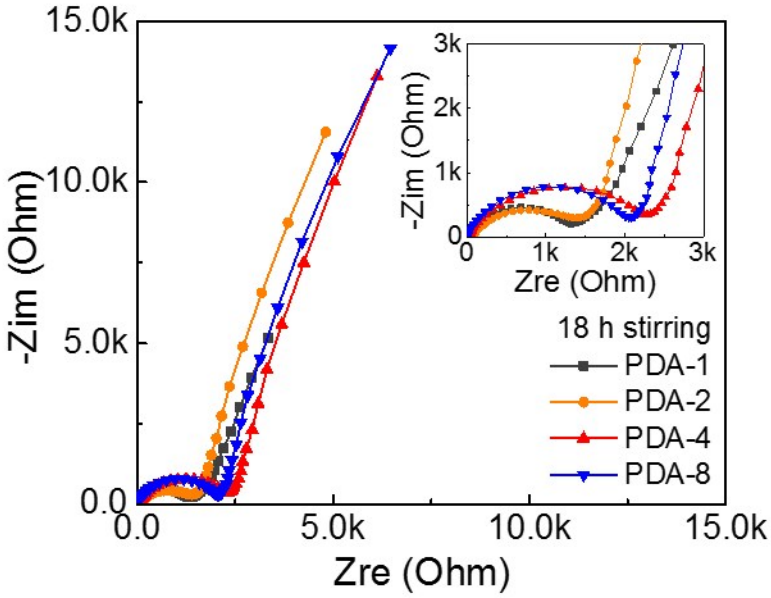

Figure S8. Nyquist plots of the hybrid electrodes (PDA-1,2,4, and 8) in fresh Li-cells from 200 kHz to 100 mHz at room temperature. The inset shows the magnified plot for the high frequency region.

Table S4. Comparison of capacities of various organic electrodes.

#	Name	Capacity (mAh/g)	Reference
1	poly(anthraquinonyl sulfide)/graphene	187 (Li)	Z. Song *et al, Nano Lett.,* **2012**, 12, 2205−2211
2	polyimide/graphene	205 (Li)	Z. Song *et al, Nano Lett.,* **2012**, 12, 2205−2211
3	poly(anthraquinonyl sulfide)	198 (Li)	Z. Song *et al, Chem. Commun.*, **2009**, 448-450
4	Polyimide/SWNT	226 (Li)	H. Wu *et al, Adv. Mater.,* **2014**, 26, 3338–3343
5	lithium 2,6-bis(ethoxycarbonyl)-3,7-dioxo-3,7-dihydro-s-indacene-1,5-bis(olate),	125 (Li)	W. Walker *et al, J. Am. Chem. Soc.,* **2010**, 132, 6517–6523
6	perylene 3,4,9,10-tetracarboxylic dianhydride based polyimide	148.9 (Na)	H. Wang *et al, Adv. Energy Mater.*, **2014**, 4, 1301651
7	benzofuro[5,6-b]furan-4,8-dione benzo[1,2-b:4,5-b']dithiophene-4,8-dione pyrido[3,4-g]isoquinoline-5,10-dione	208−234 (Li)	Y. Liang *et al, Adv. Energy Mater.,* **2013**, 3, 600–605
8	$Na_4C_8H_2O_6$	183 (Na)	S. Wang *et al, Angew. Chem. Int. Ed.,* **2014**, 53, 5892 –5896
9	$Li_4C_8H_2O_6$	223 (Li)	S. Wang *et al, Nano Lett.,* **2013**, 13, 4404−4409
10	**Polydopamine**	**217-235 (Li)** **178-213 (Na)**	**(This work)**

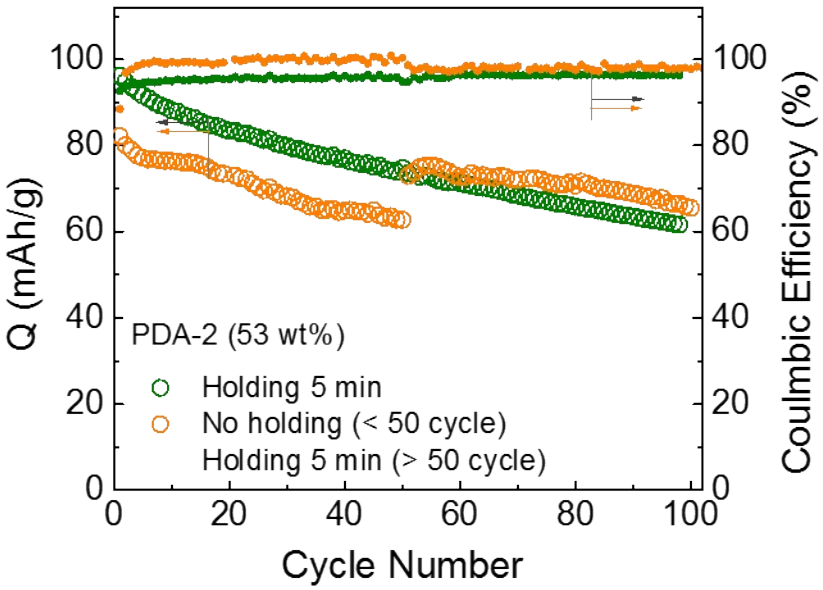

Figure S9. Cycling stabilities of the hybrid electrodes (PDA-2, 53 wt%) and their Coulombic efficiencies. The cells were cycled at 0.25 A/g up to 100 cycles.

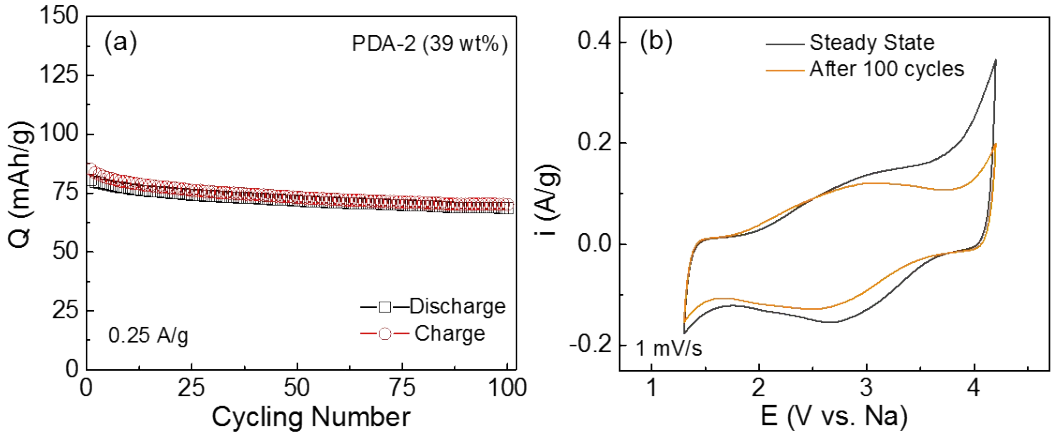

Figure S10. (a) Cycling stabilities of the hybrid electrode (PDA-2, 39 wt%) in a Na-cell. The cell was cycled at 0.25 A/g up to 100 cycles. (b) The comparison of CV scans at the initial cycle and after 100 cycles at 1 mV/s.

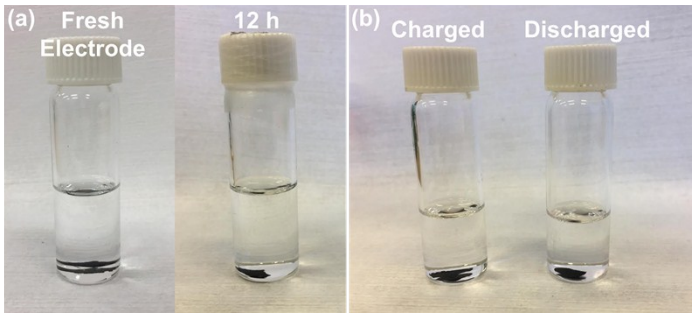

Figure S11. Dissolution tests of (a) fresh hybrid electrode and (b) charged (left) and discharged (right) electrode.

References:

1. R. Ditchfield, W. J. Hehre and J. A. Pople, *The Journal of Chemical Physics*, 1971, **54**, 724-728.
2. , Jaguar version 7.6 Schrodinger, LLC, New York, NY, 2009.
3. P. Winget, J. C. Cramer and G. D. Truhlar, *Theoretical Chemistry Accounts*, 2004, **112**, 217-227.
4. Z. Chen, D. Y. Kim, K. Hasegawa, T. Osawa and S. Noda, *Carbon*, 2014, **80**, 339-350.
5. D. Y. Kim, H. Sugime, K. Hasegawa, T. Osawa and S. Noda, *Carbon*, 2011, **49**, 1972-1979.
6. T. Liu, R. Kavian, Z. Chen, S. S. Cruz, S. Noda and S. W. Lee, *Nanoscale*, 2016, **8**, 3671-3677.
7. R. A. Zangmeister, T. A. Morris and M. J. Tarlov, *Langmuir*, 2013, **29**, 8619-8628.